Design Aspects of Bright Red Emissive Silver Nanoclusters/DNA Probes for MicroRNA Detection

Pratik Shah,[†] Andreas Rørvig-Lund,[‡] Samir Ben Chaabane,[†] Peter Waaben Thulstrup,[§] Henrik Grum Kjaergaard,[‡] Eduard Fron,[⊥] Johan Hofkens,[⊥] Seong Wook Yang,[†,*] and Tom Vosch[‡,*]

[†]Department of Plant Biology and Biotechnology, University of Copenhagen, Thorvaldsensvej 40, 1871 Frederiksberg, Copenhagen, Denmark, [‡]Nano-Science Center/ Department of Chemistry, University of Copenhagen, Universitetsparken 5, 2100 Copenhagen, Denmark, [§]Department of Chemistry, University of Copenhagen, Thorvaldsensvej 40, 1871 Frederiksberg, Copenhagen, Denmark, and [⊥]Department of Chemistry and Institute for Nanoscale Physics and Chemistry, Katholieke Universiteit Leuven, Celestijnenlaan 200F, 3001 Heverlee, Belgium

ABSTRACT

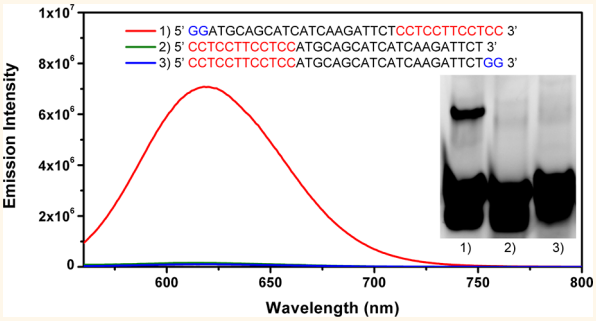

The influence of the nucleic acid secondary structure on the fast (1 h) formation of bright red emissive silver nanoclusters (AgNCs) in a DNA sequence (DNA-12nt-RED-160), designed for the detection of a microRNA sequence (RNA-miR160), was investigated. The findings show that especially the propensity for mismatch self-dimer formation of the DNA probes can be a good indicator for the creation and stabilization of red emissive AgNCs. Also, the role of the thermal stability of the secondary DNA structures (mismatch self-dimer and hairpin monomers) and the observed AgNC red emission intensity were investigated. These findings can form the basis for a rationale to design new red emissive AgNC-based probes. As an example, a bright red emissive AgNC-based DNA probe was designed for RNA-miR172 detection. The latter opens the possibility to create a variety of AgNC-based DNA probes for the specific detection of plant and animal miRNAs.

KEYWORDS: mismatch self-dimer · hairpin · DNA/AgNC probe · miRNA detection · fluorescence · silver nanoclusters · native gel electrophoresis

DNA-based silver nanoclusters (AgNCs), which have a high brightness and good photostability and are fairly inexpensive to produce, have recently provided a new prospect for the development of biolabels and molecular sensors due to the different emissive species that span the whole visible range.[1−28] A combination of the functional aspects of DNA with the spectroscopic features of DNA-encapsulated AgNCs enables the retrieval of spectroscopic information about the presence of analytes, by enhancement or quenching of the emission intensity and/or by shifting the emission wavelength. For instance, yellow emissive AgNCs in a DNA probe can be transformed into 500-fold brighter red emitting AgNCs when the probe is partially hybridized with a complementary sequence with a guanine-rich overhang.[8] Alternatively, the red emission from AgNCs in a 12 cytosine base strand is quenched by the presence of mercury ions.[29] Also, a single point mutation in a gene can be analyzed by fluorescent quenching with a DNA/AgNC probe.[30] Guo *et al.* synthesized a DNA probe (Str-C) that forms a duplex with a partial fragment of the hemoglobin beta chain (HBB) gene and has a six cytosine base loop.[30] When the Str-C binds to a normal HBB fragment, it generates no significant fluorescence, whereas upon binding to the mutated HBB fragment, substantial emission is observed. Strategies using both quenching and enhancement can also be used as demonstrated by Petty *et al.*[14] A bifunctional sensor strand with a scaffold for a silver cluster and a target recognition site were applied with a statically quenching strand to detect target DNA.[14] In the presence of a target strand, the quenching strand (which is partially complementary to the bifunctional strand) is competitively displaced, resulting in near-infrared emission. These interesting strategies can be applied to create very specific and sensitive biosensors, in which spectroscopic features are drastically altered by target recognition.

Previously, we reported a new strategy for a plant microRNA (RNA-miR160) detection using a DNA-12nt-RED-160 sensor strand that displayed unusually strong and

* Address correspondence to tom@chem.ku.dk; swyang@life.ku.dk.

Received for review June 14, 2012 and accepted September 4, 2012.

Published online September 04, 2012
10.1021/nn302633q

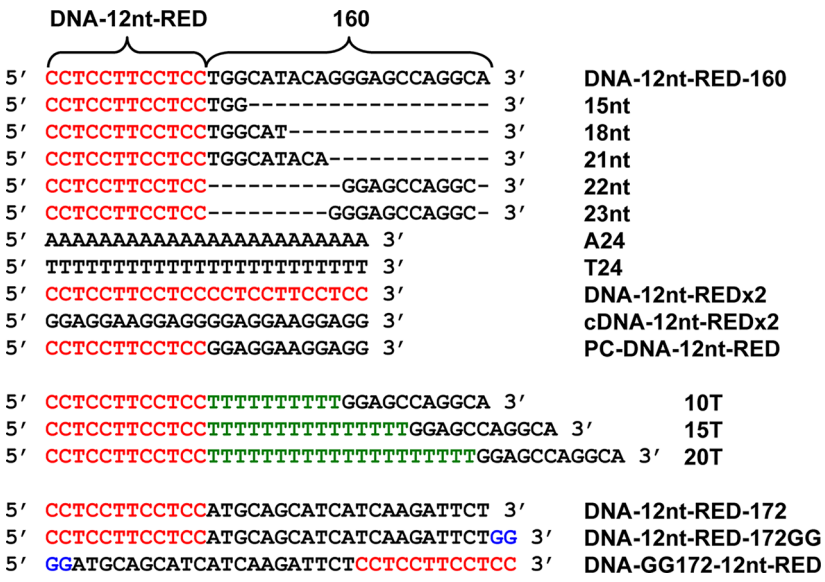

Figure 1. DNA sequences with their abbreviations used throughout the article. In red, the original red emissive AgNC creating part (DNA-12nt-RED) is given. 15nt, 18nt, 21nt, 22nt, and 23nt are shortened versions of the DNA-12nt-RED-160 probe. A24, T24, DNA-12nt-REDx2, cDNA-12nt-REDx2, and PC-DNA-12nt-RED are controls used in the gel electrophoresis and high-resolution melting experiments. 10T, 15T, and 20T are modified versions of the DNA-12nt-RED-160 probe where the middle part is replaced by an increasing section of thymine nucleotides (green). DNA-12nt-RED-172, DNA-12nt-RED-172GG, and DNA-GG172-12nt-RED are probes constructed for the RNA-miR172 detection experiments.

fast formation (1 h) of red-emissive AgNCs.[13] Like the bifunctional sensor strand mentioned earlier, the DNA-12nt-RED-160 sensor has two functional units, a 12-nucleotide part (DNA-12nt-RED) that acts as the AgNC scaffold and a 21-nucleotide target recognition site (160) for RNA-miR160 (see Figure 1 for a schematic illustration).[14] In contrast to the DNA strands by Petty *et al*. that show near-infrared emission upon target hybridization, the microRNA (miRNA) detection probe developed in our lab has a strong red emission by itself and displays a dramatic drop in the observed red emission in the presence of target miRNA.[14] In our efforts to create a series of probes to detect other miRNAs in plants, we noticed that when the RNA recognition sequence is replaced with another target recognition site, not all probes form fast, bright red emission. The latter indicated that not only the DNA-12nt-RED part but the structure of the whole probe plays an important role for the creation of the bright red emissive AgNCs. Recently, several studies have indicated that the secondary structures of the DNA scaffolds are important for AgNC formation: For instance, fluorescent AgNCs can be encapsulated by hairpin structures with 3 to 12 cytosines in the hairpin area, resulting in AgNC emission maxima ranging between 526 and 688 nm.[10] Cytosine-rich DNA sequences are also able to form intermolecular C−C base paring that allows the formation of an I-motif structure. It was reported that I-motif forming DNA sequences generate red and green emissive species in a pH-dependent manner.[4] Similarly, G-rich sequences can form a G-quadruplex structure due to the G−G base paring and host red emitting AgNCs (686 nm) in acidic conditions.[21] Interestingly, when the G-rich sequences are annealed with complementary C-rich sequences to form double-stranded DNA, the red emission shifted to near-infrared (708 nm).[21] With respect to these studies and our previous work, the fast formation of bright red emissive AgNCs in the DNA-12nt-RED-160 probe likely arises as a consequence of the specific secondary structures it can form.[13]

In order to explain why certain probes did not perform so well, modified versions of the DNA-12nt-RED-160 were studied to gain insight in the red emissive AgNC formation in the DNA-12nt-RED-160 probe. Ultimately, we show that the insight gained here for the modified DNA-12nt-RED-160 sequences allowed us to explain why other probes gave less red AgNC emission. In this paper, we chose the DNA-12nt-RED-172 probe as an example, and we show how it was redesigned to give a similar performance to the original DNA-12nt-RED-160 probe.

RESULTS AND DISCUSSION

Correlation between Structure and Observed Red AgNC Emission in DNA-12nt-RED-160-Based Probes. Our design starting point was the DNA-12nt-RED-160 probe created to detect a target RNA-miR160 sequence and which formed bright red fluorescence within 1 h after addition of $AgNO_3$ and reduction with $NaBH_4$.[13] The DNA-12nt-RED-160 probe consists of a sequence that was shown previously by Richards *et al.* to generate red emissive AgNCs (DNA-12nt-RED) and a complementary DNA part of the miRNA-160 (160) target (see Figure 1).[31] Attempts to expand this idea and create probes for detecting different miRNA sequences were not straightforward, as two out of eight different miRNA probes did not form bright red emissive AgNCs. An example of such a probe is DNA-12nt-RED-172 (see Figure 1). This probe was constructed for the

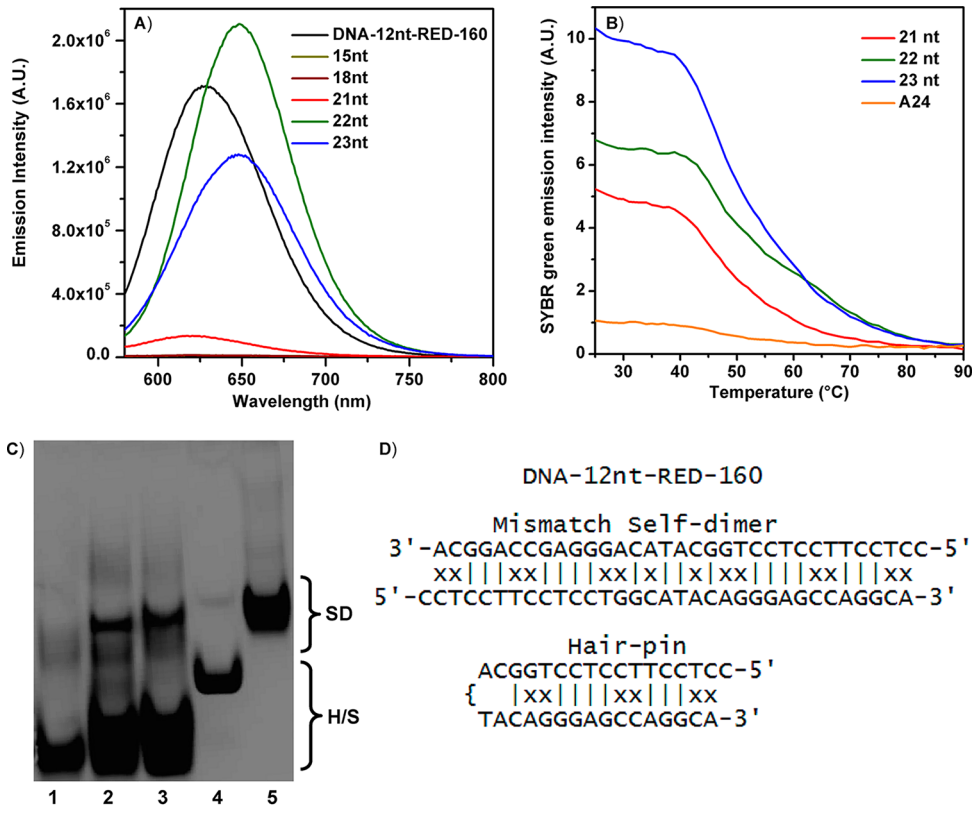

Figure 2. (A) Emission spectra of the DNA-12nt-RED-160, 15nt (close to baseline), 18nt (close to baseline), 21nt, 22nt, and 23nt. The emission spectra (excited at 560 nm) were recorded 1 h after mixing and reducing the DNA/$AgNO_3$ mixture with $NaBH_4$. (B) HRM analysis of 21nt, 22nt, 23nt, and A24. Native DNA without AgNCs was used in the HRM experiments, and the observed green emission (monitored at 510 nm) is from the added SYBR green dye. (C) Native gel electrophoresis of (1) 21nt, (2) 22nt, (3) 23nt, (4) A24, and (5) A24/T24 1:1 ratio mixture. $AgNO_3$ and $NaBH_4$ were added to all the DNA samples before running the gel electrophoresis experiment. SD: mismatch self-dimer or double-stranded DNA. H/S: hairpin and single-stranded DNA. (D) Two suggested secondary DNA-12nt-RED-160 structures of a mismatch self-dimer and a hairpin with similar base pair interaction motif.

detection of RNA-miR172 (a miRNA sequence that is important for flower development).[32] SI Figure 1 shows the red emission intensity of DNA-12nt-RED-172, 1 h after addition of $AgNO_3$ and $NaBH_4$, excited at 540 nm. The emission intensity is a factor of 10 lower than that of the DNA-12nt-RED-160 probe (see Figure 2A). This data indicated that not only the DNA-12nt-RED sequence but the structure of the whole probe play important roles for the creation of the bright red emissive AgNCs. In order to gain insight into these observed differences in red emission intensity between the DNA-12nt-RED-160 and the DNA-12nt-RED-172 and in order to find a general rationale for designing quenching-based red emissive AgNC probes for miRNA detection, a series of experiments were performed, modifying the original DNA-12nt-RED-160 probe. Figure 1 shows a series of DNA sequences of varying length, based on the original DNA-12nt-RED-160 probe sequence. As oligonucleotide length affects the tendency to form self-dimers or hairpin structures, the effect of the nucleic acid secondary structure on the obtained fluorescence properties can be investigated. The sequences 15nt, 18nt, and 21nt are versions of DNA-12nt-RED-160 shortened at the 3′ end, while for 22nt and 23nt a section in the middle of the DNA-12nt-RED-160 sequence was removed as well as the adenine at the 3′ end. Figure 2A shows the observed red emission upon excitation at 560 nm, 1 h after addition of $AgNO_3$ and $NaBH_4$ to the above-mentioned DNA sequences. Like the DNA-12nt-RED sequence, reported by Richards *et al.*, 15nt and 18nt sequences give very little fluorescence after 1 h.[31] As reported earlier, the emission from the DNA-12nt-RED sequence does however gradually increase over time.[13] Going from 18nt to 21nt, we see a noticeable increase in the observed fluorescence intensity, however still about a factor of 10 less than that obtained for the DNA-12nt-RED-160 sequence. Besides the original DNA-12nt-RED-160, also the 22nt and 23nt sequences result in high fluorescence intensity after 1 h. The emission maxima of both 22nt and 23nt are 30 nm red-shifted compared to DNA-12nt-RED-160, to a value of 650 nm. The amount of observed red emission after 1 h is clearly sequence dependent, and it is likely related to the different secondary structures that the DNA sequences can adopt in solution. The latter can also be found in previous literature reports where it has been observed that secondary structures like hairpin loops and double-stranded DNA sequences (with or without mismatches), I-motifs, and G-quadruplex are good templates for the

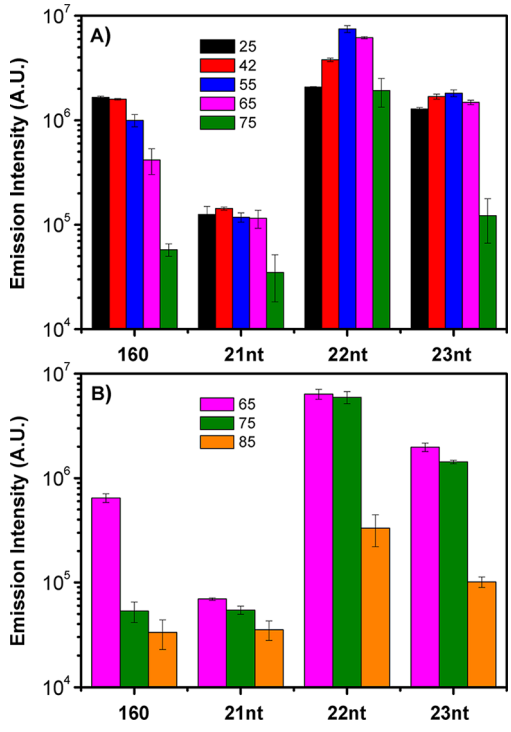

Figure 3. (A) Red emission (intensity value of the emission maximum, excited at 560 nm) from AgNCs formed with DNA-12nt-RED-160 (indicated by 160), 21nt, 22nt, and 23nt, monitored 1 h after formation at 25, 42, 55, 65, and 75 °C. (B) Red emission (intensity value of the emission maximum, excited at 560 nm) from AgNCs formed with DNA-12nt-RED-160 (indicated by 160), 21nt, 22nt, and 23nt formed for 1 h at the specified temperature of 25 °C, followed by heating the sample for 1 h at 65, 75, and 85 °C. All the DNA sequences were first denatured by heating at 100 °C for 10 min. For both (A) and (B), every data point is an average of 3 experiments, with the error bar representing the standard deviation.

formation of AgNCs.[4,6,8−11,14,21,33] Driehorst *et al.* showed that the conformation plays a critical role in the stabilization of emissive species AgNCs by electrophoretic mobility and diffusivity measurements.[11] Native gel electrophoresis of the AgNC-containing DNA sequences showed that especially the sequences that had the highest red emission intensity (22nt, 23nt, and DNA-12nt-RED-160) also contained the presence of mismatch self-dimers (see Figure 2C and Figure 4D). SI Figure 2 shows a scatter plot between the amount of mismatch self-dimer in the gel and the red AgNC emission observed after 1 h at 25 °C. The amount of mismatch self-dimer ranges between 1% and 5% for the bright red emissive AgNC-containing sequences 22nt, 23nt, and DNA-12nt-RED-160. For 21nt no clear self-dimer mismatch band was seen. In Figure 2C also two controls were added, A24 and a 1:1 ratio mixture of A24/T24, both with $AgNO_3$ and $NaBH_4$ reactants added before addition to the gel. As expected, A24 shows up as a single-stranded structure, while the A24/T24 mixture shows up as a double-stranded DNA structure. In order to investigate the strength of the secondary structures and the amount of interacting base pairs, a high-resolution melting (HRM) analysis was performed. The HRM method was developed to detect a single base change in duplex DNA molecules with extremely high resolution. In the HRM experiments, SYBR green, which is added to the DNA samples, becomes fluorescent upon intercalation in double-stranded DNA segments. Hence the drop in SYBR green emission can be used to monitor the amount of interacting base pairs and the temperature stability of hairpin stem regions and other base pair structures, *e.g.*, like in mismatch self-dimers, upon heat denaturation. In the HRM experiments, $AgNO_3$ and $NaBH_4$ were not added to the DNA sequences. SI Figure 3 shows two control experiments clearly demonstrating that the HRM can be used for analyzing the temperature stability of the short DNA sequences used in this article. HRM experiments for A24, T24, a 1:1 ratio mixture of A24 and T24 (A24/T24), DNA-12nt-REDx2, cDNA-12nt-REDx2, and a 1:1 ratio mixture of DNA-12nt-REDx2 and cDNA-12nt-REDx2 (DNA-12nt-REDx2/cDNA-12nt-REDx2) were performed. Only in the case for A24/T24 and DNA-12nt-REDx2/cDNA-12nt-REDx2, where a mixture of complementary strands is present, do we see high SYBR green emission values as expected. Figure 2B shows the HRM curve for 21nt, 22nt, and 23nt, while the HRM curve for DNA-12nt-RED-160 can be found in Figure 4C. A first observation is that the signal intensity for DNA-12nt-RED-160 is much higher than for 21nt, 22nt, and 23nt. This is not too surprising since DNA-12nt-RED-160 is much longer than 21nt, 22nt, and 23nt, hence could potentially accommodate more SYBR green within its structure. More interesting is to compare 21nt, 22nt, and 23nt, which are close to each other in length. Despite the fact that 22nt and 23nt give the highest initial SYBR green intensity at 25 °C, the value for 21nt is not that much lower, indicating that the number of interacting base pairs is not so dramatically different compared to 22nt and 23nt. In SI Figure 4, the normalized HRM curves for 21nt, 22nt, 23nt, and DNA-12nt-RED-160 are given. In this way we can directly compare the temperature stability of the four DNA sequences. In this particular case, a correlation can be observed in which the sequences that seem to generate the most red AgNC emission in Figure 2A also have the highest temperature stability. However, the fact that 21nt had a substantially lower amount of mismatch self-dimer (as can be seen from the native gel electrophoresis picture in Figure 2C) and a much lower red AgNC emission indicates that the presence of mismatch self-dimer structures can be a good indicator for the presence of red emissive AgNCs. The possibility that red emissive AgNCs can be stabilized by mismatch self-dimers is a novel concept and differs from previously reported AgNC emission in mismatch dimers, where two nonidentical DNA strands are required.[18] Based on the initial findings from the shortened versions of the DNA-12nt-RED-160 probe, a correlation can be drawn in which increased emission from red emissive AgNCs seems to increase when more secondary structures are present and when

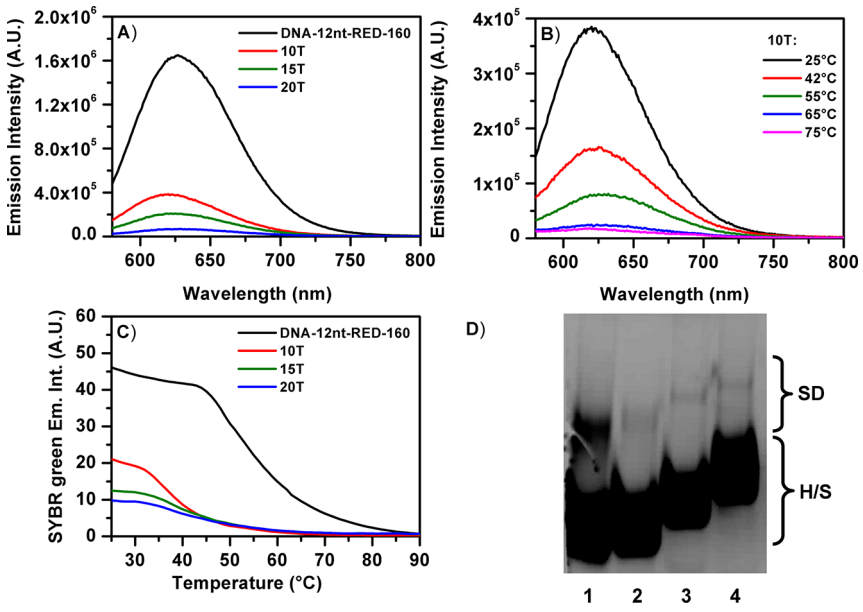

Figure 4. (A) Emission intensity of red emitting AgNCs formed with 10T, 15T, and 20T compared to DNA-12nt-RED-160, 1 h after creation at 25 °C. (B) Emission intensity of red emitting AgNC formed by 10T, 1 h after creation at the specified temperatures: 25, 42, 55, 65, and 75 °C. (C) HRM analysis of DNA-12nt-RED-160, 10T, 15T, and 20T (no AgNCs were present here). (D) Native gel electrophoresis of (1) DNA-12nt-RED-160, (2) 10T, (3) 15T, and (4) 20T. $AgNO_3$ and $NaBH_4$ were added to all the DNA samples before running the gel electrophoresis experiment. SD: mismatch self-dimer or double-stranded DNA. H/S: hairpin and single-stranded DNA.

these DNA structures have a higher temperature stability. Despite the fact that the presence of a mismatch self-dimer band is a good indicator for the formation of bright red emissive AgNCs, the latter does not necessarily prove that most of the red emissive AgNCs are stabilized in mismatch self-dimer structures. The presence of a mismatch self-dimer band in the native gel electrophoresis could also indicate the presence of stable mismatch hairpin structures with a similar base pair interaction motif. Figure 2D shows that one can construct a hairpin structure that is similar to the right-hand side of the mismatch self-dimer, suggesting that if a stable mismatch self-dimer can be formed, a similar mismatch hairpin structure corresponding to half the mismatch self-dimer could also be possible. It seems logical to assume that if the base pair interation motif is similar in both cases, they would interact in a similar way with the AgNCs. The latter, combined with the much larger hairpin/single-strand band in the native gel experiments, suggests that we cannot fully exclude the possibility that a significant fraction of the emissive AgNCs are in the hairpin region. However, we cannot exclude that the gel running conditions could physically denature a portion of the mismatch self-dimer band and, as a result, under-represent the amount of mismatch self-dimers that are present in solution. A clear proof that self-dimers are good hosts for stabilizing AgNCs is given in SI Figure 5. PC-DNA-12nt-RED (see Figure 1) can form a perfect self-dimer with itself. The full emission scan shows the presence of bright red emissive AgNCs after 1 h, and the native gel electrophoresis shows only a single self-dimer band, excluding the possibility of the AgNCs residing in the hairpin for this particular DNA sequence. Upon heat denaturing at 70 °C or higher, the red emission disappears, and when running a native gel electrophoresis of the heat-denatured PC-DNA-12nt-RED, one can see that the self-dimer band has virtually disappeared. Although the perfect self-dimer (PC-DNA-12nt-RED) gave very clear-cut results, from an application point of view, we do not want the interactions of the DNA probe with itself to be too strong, potentially blocking the hybridization with the microRNA target. Therefore the mismatch concept is preferred for creating red emissive AgNCs.

A way to gain more insight into which specific secondary structures (base pair interaction motif) are more thermodynamically favorable is by using computational molecular biology programs. Although programs such as Autodimer and Mfold can predict secondary structures of mismatch self-dimers and hairpin structures with corresponding melting temperature (T_m) and ΔG values, these results are not very representative for the DNA/AgNC complex due to the effect that metal clusters and metal cations have on the structure of nucleic acids, and therefore we do not rely here on their predicted stabilities.[34,35] For example several reports show that silver ions can promote C−Ag−C base pairing and increase the T_m value of hairpin and mismatch self-dimer structures.[18,36,37]

Also, it is interesting to note that in contrast to bright emission formed from self-dimer structures (or double-stranded oligonucleotide sequences, with or without mismatches), DNA−RNA hybrids do not generate fluorescent AgNCs (at least not for several sequences tested so far).[8,12,13,38] It was shown previously

that RNA by itself is capable of forming fluorescent AgNCs; however SI Figure 6 shows that the target miRNAs that we used (RNA-miR160 and RNA-miR172) do not form red emissive AgNCs.[39] The absence of red emissive AgNCs in the DNA−RNA hybrids could be due to the different conformation the DNA−RNA hybrid adopts.

Temperature-Dependent Creation of AgNCs with DNA-12nt-RED-160-Based Probes. In the previous section, the temperature stability for the DNA-12nt-RED-160-based probes was determined by HRM. However, the HRM experiments were performed on native DNA sequences, and therefore it is important to determine the temperature stability of the AgNC-containing DNA samples. For this, the AgNCs were created at preset temperatures and the red emission intensity was monitored after 1 h at this temperature. The predicted outcome is that at elevated temperatures (above the T_m values for certain secondary structures), a significant drop in the observed emission intensity should be observed, due to secondary structure denaturation. All DNA samples were initially denatured at 100 °C for 10 min and subsequently cooled to preset temperatures before $AgNO_3$ and $NaBH_4$ addition. The results at different preset temperatures can be seen in Figure 3A. The effect of creating the clusters at higher temperatures differs depending on the sequence: For DNA-12nt-RED-160, a steady drop is observed for the red emitting AgNCs when created at increasing temperatures. From 25 to 42 °C only a minor drop is observed. At 55 °C (40% drop) and 65 °C (75% drop), significant drops in the emission intensity are observed. At 75 °C, most of the emission disappears. For 22nt and 23nt, the fluorescence intensity increases from 25 to 55 °C, but AgNC formation above 55 °C results in lower fluorescence intensity. The observed results of 22nt and 23nt, where increased emission is observed when increasing the temperature from 25 to 55 °C, might look strange at first sight. In an attempt to denature structures with low T_m values (below 55 °C) we seem to create more emission. A possible explanation can be found in the fact that the formation of red emissive AgNCs for the 22nt sequence, when monitored at 25 °C, reaches its maximum intensity slower than for DNA-12nt-RED-160. SI Figure 7 shows that DNA-12nt-RED-160 reaches its maximum emission intensity within 1 h, while a steady increase is observed for 22nt over 5 h. One can assume that for 22nt an increase in the temperature accelerates the formation of red emitting AgNCs and that the secondary structures that stabilize the AgNCs in 22nt are more thermally stable. For 23nt, a similar effect to that for 22nt can be observed, however less pronounced. This correlates well with the lower increase of the red emission as a function of time (SI Figure 7). For 21nt the temperature effect on the formation of the red emitting AgNCs seems minimal from 25 to 65 °C, whereas at 75 °C, a drop can be observed for 21nt. Also here, one could argue that the lower temperature stability compensates the increased creation speed of red emission at higher temperatures. However, a more likely explanation could be that the DNA-12nt-RED region in 21nt is not (fully) part of the base interacting region; hence the DNA-12nt-RED region behaves more like a single-strand scaffold. The latter could explain not only the lower overall red emission and similar HRM results to 22nt and 23nt but also the limited temperature effect when increasing the temperature from 25 °C to 65 °C.

In an alternative set of experiments, AgNCs were synthesized, left at 25 °C for 1 h, and subsequently heated to 65, 75, and 85 °C for 1 h (see Figure 3B). Red emission intensities were found similar to those in Figure 3A for all four sequences at 65 °C. The biggest change compared with the data in Figure 3A is that for 22nt and 23nt the second procedure gives substantially higher emission intensities at 75 °C. This indicates that initial production of the AgNCs at lower temperatures in these two sequences has an overall stabilizing effect on red AgNC emission and probably the secondary structure. This is also to a lesser extent the case for 21nt. It is unclear from our data why this is not the case for DNA-12nt-RED-160. The results from the temperature studies show that it is not straightforward to correlate the results obtained from the HRM melting experiments with the results when AgNCs are present (*e.g.*, 22nt and 23nt). The dynamical process of AgNC creation and conversion can interfere with the interpretation of the secondary structure stability determination, when using AgNC emission as a readout.

Secondary Structure Destabilization in the DNA-12nt-RED-160 Probe by Introduction of Thymine Units. The native gel electrophoresis experiments, presented in Figure 2C, indicated that DNA sequences where mismatch self-dimers are present correlated with high red AgNC emission. Therefore, in a next step we wanted to investigate what would happen if we disrupted the possibility of forming mismatch self-dimers. For this, 10 (10T), 15 (15T), and 20 (20T) thymine bases were added in the middle of the DNA-12nt-RED-160 sequence (see Figure 1). The native gel electrophoresis pictures in Figure 4D confirm that when a long T segment is added in the middle of the DNA-12nt-RED-160 probe, the amount of mismatch self-dimers drops dramatically. Compared to DNA-12nt-RED-160, replacement of the central part with 10, 15, and 20 thymines leads to less red emission intensity from the DNA-stabilized AgNCs (Figure 4A shows the red emission with 560 nm excitation as observed 1 h following formation of AgNCs). The temperature stability of 10T, 15T, and 20T was determined by HRM analysis (see Figure 4C). The initial SYBR green intensity and the temperature stability of DNA-12nt-RED-160 are substantially higher than for 10T, 15T, and 20T. When the number of thymine bases increases from 10T to 20T, a steady drop can be

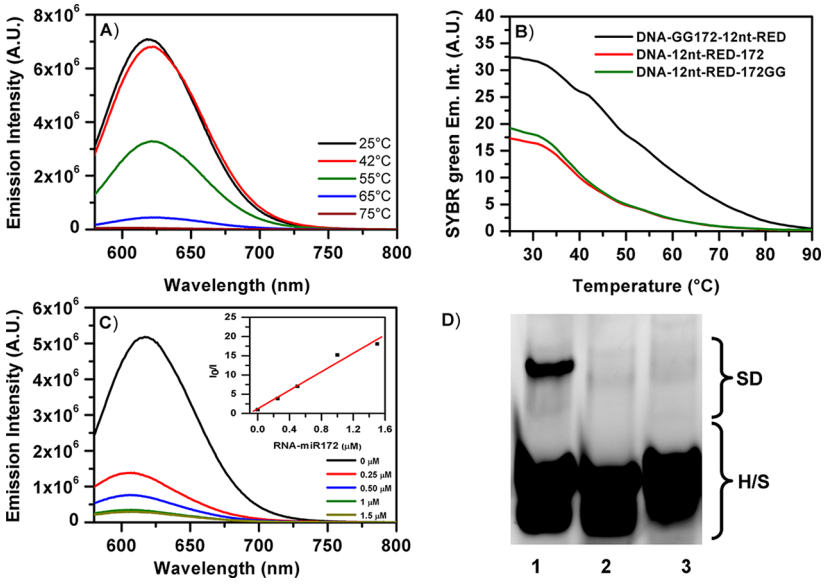

Figure 5. (A) Emission spectra of DNA-GG172-12nt-RED, excited at 540 nm, recorded 1 h after creation at the specified temperatures: 25, 42, 55, 65, and 75 °C. (B) Emission spectra of DNA-12nt-RED-172 (black curve) and DNA-12nt-RED-172GG (red curve) excited at 540 nm, recorded 1 h after creation at 25 °C. (C) Fluorescence intensity of the AgNCs formed after addition of $AgNO_3$ and $NaBH_4$ to a mixture containing 1.5 μM DNA-GG172-12nt-RED probe and RNA-miR172 target in a concentration ranging from 0 to 1.5 μM. The fluorescence spectra were recorded, exciting at 560 nm. The inset shows the Stern–Volmer plot. (D) Native gel electrophoresis of (1) DNA-GG172-12nt-RED, (2) DNA-12nt-RED-172, and (3) DNA-12nt-RED-172GG. SD: mismatch self-dimer or double-stranded DNA. H/S: hairpin and single-stranded DNA.

observed in the initial SYBR green intensity at 25 °C, indicating that the number of interacting base pairs drops. Figure 4B shows the temperature-dependent creation of red emitting AgNC for 10T. In this particular case, the drop in the red AgNC emission in Figure 4B correlates well with the drop in the SYBR green emission observed in Figure 4C, indicating that the disappearance of the red AgNC emission is linked to the denaturation of the secondary structures in 10T (see SI Figure 8). This means that the interfering effects from different AgNC creation and conversion rates at higher temperatures are minimal here. As a control we measured also the time-dependent evolution of red emission from 10T-based AgNCs. SI Figure 7 shows that the creation of red emissive AgNCs does not change significantly over a period of 5 h; hence we can use the drop in red emission at elevated temperatures to infer information about the stability of the secondary structures (based on the native gel electrophoresis picture in Figure 4D, most likely hairpin or single-stranded structures in this case).

The results of Figure 4 clearly show that the introduction of a long thymine segment, which especially hinders self-dimer formation, has a large impact on the intensity of the observed red emission and on the temperature stability. The results also show again that the sequence propensity for mismatch self-dimer formation is a good indicator for the presence of red emissive AgNCs.

Proof of Concept: Design of a Bright Red Emissive miR172-Inspired Probe. On the basis of the findings of the modified DNA-12nt-RED-160 probes, we looked back at our DNA-12nt-RED-172 probe and tried to rationalize why little red AgNC emission was observed. Because high red emissive AgNC formation in the modified DNA-12nt-RED-160 probes was likely related to the possibility of forming stable mismatch self-dimers and hairpins, native gel electrophoresis experiments were performed on DNA-12nt-RED-172, and the result is shown in Figure 5D. Figure 5D shows that DNA-12nt-RED-172 forms no significant mismatch self-dimer structures. This confirms the previous results: Only when a clear mismatch self-dimer band is present is a high red emission observed. In order the increase the probability of forming mismatch self-dimers, we inverted the positions of the DNA-12nt-RED and 172 parts and added two guanine bases at the 5′ end. This probe, called DNA-GG172-12nt-RED, did indeed show a significant amount of mismatch self-dimers in native gel electrophoresis experiments (see Figure 5D and SI Figure 2). Figure 5A shows that the DNA-GG172-12nt-RED probe has more red AgNC emission after 1 h at 25 °C than the DNA-12nt-RED-160 probe. Unlike DNA-12nt-RED-160, DNA-GG172-12nt-RED does not reach its maximum emission intensity within 1 h (see SI Figure 7). On this basis we expected, similar to the 22nt case, that creating the AgNCs at higher preset temperatures would lead to more red emission. Interestingly, as can be seen in Figure 5A, creation of red emissive AgNCs for DNA-GG172-12nt-RED at 42 °C does not give an increase in emission intensity (it stays more or less constant). A likely explanation could be that the T_m values of the secondary structures that stabilize the red emissive AgNCs are lower and that the increased formation speed for the AgNCs at higher temperatures could be balanced out by the destabilizing effect of the lower T_m value structures. From

55 °C the red emission intensity for DNA-GG172-12nt-RED starts to drop dramatically. As a control we also created DNA-12nt-RED-172GG in which two guanines were added at the end of the DNA-12nt-RED-172 sequence. This control shows that the addition of the guanines by itself does not cause the formation of a mismatch self-dimer band and increased red AgNCs emission by itself; however in DNA-GG172-12nt-RED it does because there it helps to stabilize the secondary structures (mismatch self-dimer and hairpin). Figure 5D shows that for DNA-12nt-RED-172GG no mismatch self-dimer band is present and also a similar low red AgNC emission to that for DNA-12nt-RED-172 is observed (see SI Figure 1). For all three probes (DNA-12nt-RED-172, DNA-12nt-RED-172GG, and DNA-GG172-12nt-RED) HRM experiments were performed, and the results are given in Figure 5B. Both DNA-12nt-RED-172 and DNA-12nt-RED-172GG show a lower initial SYBR emission at 25 °C and have a lower temperature stability compared to DNA-GG172-12nt-RED (see Figure 5B). Like for DNA-12nt-RED-160, the experiments here show again a correlation between high red emissive AgNC formation and structures that can form a mismatch self-dimer and temperature-stable secondary structures. SI Figure 9 shows a comparison between the temperature stability of DNA-12nt-RED-160 and DNA-GG172-12nt-RED. The secondary structures of both have a high temperature stability, but the drop is much more gradual for DNA-GG172-12nt-RED than DNA-12nt-RED-160.

The efficiency of the new DNA-GG172-12nt-RED probe was also tested for its ability to detect target RNA-miR172. Figure 5C shows that the DNA-GG172-12nt-RED performance is similar to previously reported DNA-12nt-RED-160.[13] In the inset in Figure 5C, the I_0/I (I_0 and I are the emission intensity value without and with addition of RNA-miR172, respectively) intensity *versus* RNA-miR172 target concentration is given and was fitted with a linear function that has a slope of 12 ± 0.6. The latter results in a K_D^{-1} RNA-miR172 target concentration of 82 nM, at which the fluorescence is at 50%. The miR172 quenching experiments with the redesigned DNA-GG172-12nt-RED probe clearly show that the insight from the experiments with the modified DNA-160-12nt-RED probe enabled the rational redesign of DNA-12nt-RED-172 to give the same excellent performance as the DNA-160-12nt-RED probe. Also we tested the specificity of the DNA-GG172-12nt-RED probe with five miRNA targets, and we found a similar performance to that reported previously for the DNA-160-12nt-RED probe.[13] The results can be seen in Figure 6. The RNA-miR172 target has the largest effect on I_0/I ratio (a 6 times drop in the fluorescence intensity), while the presence of RNA-miR160, RNA-miR163, RNA-miR166, or RNA-hsa-miR-21 target has only a limited effect on the observed fluorescence intensity of the DNA-GG172-12nt-RED probe (a maximum 2 times drop). We foresee that this approach will be the foundation for the construction of a range of sequence-specific miRNA probes.

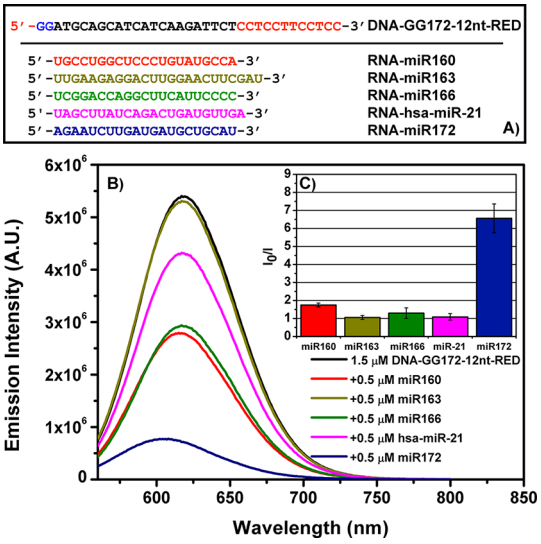

Figure 6. (A) Sequences of the DNA-GG172-12nt-RED probe and five miRNA targets: RNA-miR160, RNA-miR163, RNA-miR166, RNA-hsa-miR-21, and RNA-miR172. (B) Emission spectra (excited at 540 nm) of 1.5 μM DNA-GG172-12nt-RED probe (black curve) and mixtures of 1.5 μM DNA-GG172-12nt-RED probe with 0.5 μM RNA-miR160 target (red curve), RNA-miR163 target (dark yellow curve), RNA miR166 target (green curve), RNA-has-miR21 target (pink curve), and RNA-miR172 target (blue curve). (C) I_0/I values of the fluorescence intensity of the AgNC when adding 0.5 μM target miRNA sequences to 1.5 μM DNA-GG172-12nt-RED probe. The values are the average of 3 measurements each.

Photophysical Characterization of the Bright Red Emissive Probes. We have measured absorption and circular dichroism (CD) spectra and fluorescence excitation and emission spectra and performed time-correlated single photon counting experiments in order to investigate in detail the photophysical properties of the bright red emissive AgNC-forming DNA sequences. Figure 7A shows the steady-state absorption spectra for DNA-12nt-RED-160, DNA-GG172-12nt-RED, 22nt, and 23nt. We here primarily discuss the absorption peaks from 500 nm and higher, since these are mostly responsible for the red emitting properties of the AgNCs. However, for all sequences, several other absorption peaks are also observed throughout the visible region below 500 nm. For 22nt, two absorption maxima can be identified in the region above 500 nm, one around 500 nm and one at 580 nm. The peaks at 500 and 580 nm can be identified in the fluorescence excitation spectra at similar positions (see SI Figure 11), indicating that we have at least two types of AgNCs or AgNC environments that yield red emission (both possibilities will be further referred to as AgNC species). The emission spectra of 22nt show two well-defined emission peaks, one centered at 600 nm and one at 660 nm. The 600 nm emission peak shifts to the 660 nm peak upon increasing the excitation wavelength, indicating that we are spectrally moving from exciting

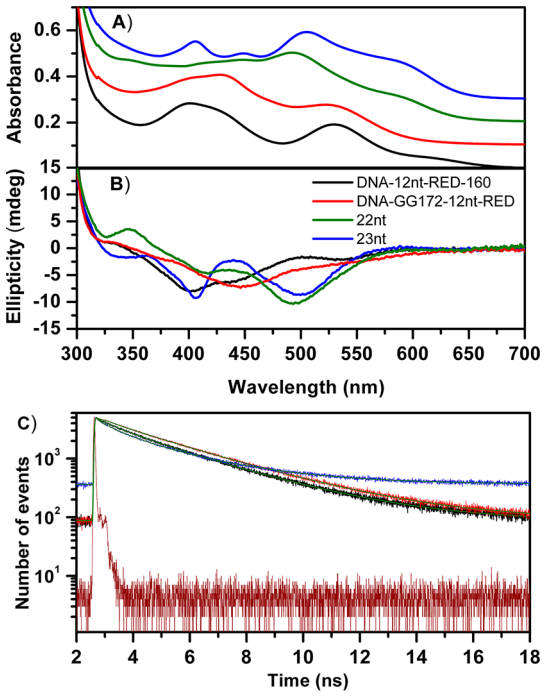

	α_1	f_1	τ_1	α_2	f_2	τ_2	α_3	f_3	τ_3
DNA-12nt-RED-160	0.26	0.02	0.14	0.20	0.12	1.14	0.54	0.86	2.89
DNA-GG172-12nt-RED	0.13	0.01	0.19	0.18	0.11	1.50	0.69	0.88	3.11
21nt	0.31	0.03	0.16	0.29	0.20	1.09	0.40	0.77	2.92

Figure 7. (A) Absorption spectra of DNA-12nt-RED-160, DNA-GG172-12nt-RED, 22nt, and 23nt (concentration 15 μM). (B) Circular dichroism spectra for DNA-12nt-RED-160, DNA-GG172-12nt-RED, 22nt, and 23nt (concentration 15 μM). (C) Time-correlated single photon counting experiments for DNA-12nt-RED-160 (1.5 μM, black curve), DNA-GG172-12nt-RED (1.5 μM, red curve), 21nt (3 μM, blue curve), and IRF (brown curve). The samples were excited at 561 nm, and the fluorescence decay was monitored at 600 nm. Table with the values from a triexponential fit of the fluorescence decays of the 3 samples. Fluorescence decay times (τ) in nanoseconds, normalized amplitudes (α), and fractional (f) contributions to the overall fluorescence intensity.

one type of AgNC species to another. Once the emission maximum is at 660 nm, it does not shift further to higher wavelengths. The circular dichroism spectrum for 22nt, however, displays a negative peak, centered close to 500 nm, corresponding well with the peak at 500 nm in the absorption spectrum. It seems that the absorption peak (which matches the fluorescence excitation peak that gives the highest red emission) at 580 nm does not appear in the CD spectrum. This indicates that the two AgNC species absorbing at 500 and 580 nm are structurally distinct, yielding some information about the location of the AgNC. Wu *et al.* suggested that AgNCs can be formed at different locations inside or at the side of a stretch of double-stranded DNA.[40] When inside the DNA double strand it is possible that due to the chiral surroundings of the DNA, the AgNC absorbance shows up with a chiral signature in the CD spectrum, and this type of behavior was recently demonstrated for a near-infrared emitter by Petty *et al.*[5] Thus here it could be that one type of red emitting AgNC species is surrounded by the chiral DNA and displays induced CD, while the other does not or does so to a much smaller degree. A similar result is observed for 23nt. Clearly, two absorption peaks are seen in the region above 500 nm (at 510 and 580 nm), with only one peak showing up around 500 nm in the CD spectrum. A difference between 22nt and 23nt is that the absorption peak close to 500 nm is about 10 nm red-shifted compared to 22nt. Also the fluorescence excitation spectra for 23nt do not as clearly show two peaks like 22nt (see SI Figure 12), but the emission spectra shift slightly upon increasing the excitation wavelength. The fluorescence excitation spectra give a maximum for red emission at 580 nm, which corresponds again with the absorption peak around 580 nm. Since we observe a continuous shift of the emission spectra, there could be more than two emissive AgNC species present. Again, the AgNC species responsible for the largest amount of red emission does not seem to be very CD active. This shifting of the emission maxima is even more pronounced for DNA-12nt-RED-160 (see SI Figure 10). In the absorption spectra of DNA-12nt-RED-160, two maxima can be seen at 525 and 620 nm. In the CD spectrum however, again only one negative peak clearly appears close to 525 nm. The fluorescence excitation spectrum gives the maximum red emission at 600 nm; however we noticed that there are variations in where the maximum is observed. In some experiments the maximum is at 580 or 560 nm. Together with the shifting in the emission spectra we can conclude that there are definitely more than two types of red emitting AgNC species present in DNA-12nt-RED-160. Besides this, also a bit of green emission (with an emission maxima at 540 nm; see SI Figure 10) is generally observed, as was also reported previously.[13] DNA-GG172-12nt-RED looks different from the previous three sequences. In the absorption spectrum, only one distinct peak can be observed, centered at 525 nm. This is also clearly reflected in the fluorescence excitation spectra, which show maxima that are all centered close to 540 nm (see SI Figure 13). The emission spectra (see SI Figure 13) show emission maxima close to 625 nm that do not seem to shift when increasing the excitation wavelength as seen for DNA-12nt-RED-160. This could indicate that there is only one type of emissive red AgNC species present or that the different AgNC species are spectrally very similar. The CD spectra show no defined negative peak around 525 nm, only a slope that extends from 625 nm until 480 nm. Although the nature of this slope is unclear, it seems that again the absence of a clear peak in the CD spectrum corresponding to the maximum of the most intense excitation spectra indicates that the larger contribution to the red emission is from AgNC species that are not strongly CD active.

Time-correlated single photon counting experiments were also performed, and the results are given in Figure 7C. The fluorescence decays were recorded, exciting the samples at 561 nm and detecting the

emission at 600 nm. Fitting the fluorescence decay curve by instrument response function (IRF) deconvolution required the use of a triexponential function (see SI Figure 14 for comparison between one-, two-, and triexponential fit). The three obtained decay times from the fit were similar for DNA-12nt-RED-160, DNA-GG172-12nt-RED, and 21nt, with values around 0.15 ns, 1.1 ns (DNA-GG172-12nt-RED had a slightly higher value around 1.5 ns), and 3 ns. The amplitudes of each of the decay components were different for each of the compounds however. The major contributor to the observed fluorescence is coming from the component with a decay time around 3 ns. The amplitude of the 3 ns component was the lowest for 21nt (which showed no significant mismatch self-dimer band in Figure 2) with a value of 0.4, while it was significantly higher for DNA-12nt-RED-160 and DNA-GG172-12nt-RED (0.54 and 0.69, respectively). The multiexponential fluorescence decay is different from the monoexponential decay of 12nt, reported by Richards *et al*., who found a single decay time of 2.23 ns.[31] An explanation for this is that 12nt has a low probability to form secondary structures such as hairpin or self-dimer structures and the emission coming from 12nt is due to a specific position of the AgNCs within the 12nt. The latter indicates that the multiple decay components for the red emitting AgNCs might come from their position in different surroundings (in either the self-dimer or hairpin structures). The latter also hints that the presence of a counterpart to the 12nt area (either as a mismatch self-dimer or as the stem region in a hairpin structure) is what determines the spectral properties and brightness of the AgNC. Additional support for this idea can be found in the work by Yeh *et al*.,[8] who attached a yellow emissive sequence (as reported by Richards *et al*.) to a probe sequence.[31] Upon binding of a partial complementary DNA sequence (and even for the perfect complementary sequence) to the probe sequence, bright red emission was observed.

CONCLUSION

Here, we have shown a series of findings that support a model where the propensity for mismatch self-dimer formation is an indicator for the ability to form bright red emitting AgNCs in the modified DNA-12nt-RED-160 DNA sequences. While unstructured 12nt, 15nt, and 18nt showed lower, single-strand-like emission intensities, 22nt and 23nt, which can form mismatch self-dimers, showed higher emission than DNA-12nt-RED-160 at their maximum excitation (580 nm). When stable mismatch self-dimers can be formed, corresponding hairpin structures similar to half the mismatch self-dimer will also likely be stable. The latter, combined with the limited amount (1−5%) of mismatch self-dimer band in the native gel experiments, suggests that we cannot exclude that a significant fraction of the emissive AgNCs are in the hairpin region. However, the amount of the mismatch self-dimer could be under-represented in the gel due to denaturing while running the experiment. A clear proof that self-dimers are good hosts for stabilizing AgNCs was given by PC-DNA-12nt-RED, which can form a perfect self-dimer with itself. Here only a self-dimer band was observed in the gel electrophoresis experiments, and bright red emissive AgNCs were formed in solution. The temperature studies showed that the results obtained from the HRM experiments can differ from the results when using AgNC emission as a readout for secondary structure stability (*e.g*., 22nt and 23nt). The latter is due to the dynamical AgNC creation and conversion process and the additional stabilizing effect the AgNC can have on the secondary structure of the DNA. To confirm the importance of secondary structure and the possibility to form mismatch self-dimers, 10 bases in the middle of the DNA-12nt-RED-160 probe were replaced with a series of thymine bases. The results confirmed again that the reduction in secondary structures also led to a reduction in the amount of red emissive AgNCs. On the basis of the previous results, we rearranged the sequence of the low-emissive DNA-12nt-RED-172 probe to increase formation of secondary structure. The redesigned DNA-GG172-12nt-RED showed a dramatic increase in red emission, which strongly supports our rationale. Furthermore, we showed that target RNA-miR172 efficiently quenched our DNA-GG172-12nt-RED probe, providing a rationale for the design of other DNA/AgNC probes for miRNA detection.

EXPERIMENTAL SECTION

$AgNO_3$ (99.9999%) and $NaBH_4$ (99.99%) were purchased and used as received from Sigma Aldrich. MiRNA targets and DNA probes were commercially synthesized by Eurofins (HPLC purified). The DNA sequences used in the publication are described in Figure 1. All probes at 15 μM were dissolved in autoclaved Milli-Q water, then denatured at 100 °C for 10 min and immediately transferred to heat blocks that were adjusted to preset temperatures (25, 42, 55, 65, and 75 °C) to anneal the DNA structures for 20 min. No pH buffer or salt was added to the Milli-Q water. SI Figure 15 shows no significant influence on the red AgNC emission was observed for DNA-12nt-RED-160 in a pH range from 6 to 9.5 and upon addition of up to 1 mM $NaNO_3$ before measurement (10 times dilution). Then, to make fluorescent AgNCs, the DNA probes were mixed with $AgNO_3$ (250 μM) and $NaBH_4$ (250 μM) (1:17:17) to a final volume (50 μL) within the heat blocks (for example, the experiments presented in Figure 2A and Figure 3A). For the experiments presented in Figure 3B, DNA/AgNCs were generated at 25 °C for 1 h and then transferred to the heat denaturing temperatures (65, 75, and 85 °C) for 1 h. Time-dependent emission measurements were performed with five separately prepared samples at 25 °C for each measurement point (measured at 1, 2, 3, 4, and 5 h after creation). For the miRNA detection assay, we added various concentrations of RNA-miR172

(0.2 to 15 μM) to DNA-GG172-12nt-RED (15 μM) and incubated for 20 min at 25 °C. For the miRNA specificity assay, 5 μM of different miRNAs were added to 15 μM DNA-GG172-12nt-RED and incubated for 20 min at 25 °C. Then, to make fluorescent AgNCs, the DNA probes were mixed with $AgNO_3$ (250 μM) and $NaBH_4$ (250 μM) (1:17:17) to a final volume (50 μL). For all the fluorescence excitation and emission spectra recorded for the above-mentioned experiments, the samples were diluted with 450 μL (final DNA concentration: 1.5 μM) of preheated Milli-Q water with the same temperature as the sample before the measurements were performed with a fluorimeter (Horiba Jobin Yvon, Fluoromax-4) in 10 mm plastic disposable cuvettes. To prevent any temperature changes while moving from heat blocks to fluorimeter, empty plastic cuvettes also were preheated at the specific temperature for 30 min. As a control, the fluorescence from several samples measured in plastic cuvettes was compared with the quartz cuvettes, but showed no significant difference between them. The values reported in Figure 3A and B are averages of six measurements. When creating AgNCs with DNA sequences for which the emission keeps increasing dramatically in the first hours, such as DNA-GG172-12nt-RED, significant differences in the initial value after 1 h of the emission intensity can be observed. Also the full spectral recordings in SI Figures 10−13 were started at 1 h after preparation, but due to the significant recording time, the spectra might display higher emission values compared to the time-dependent measurement in SI Figure 7, where only one emission spectrum was recorded.

To detect the mismatch self-dimer structures from the DNA/AgNC compounds, gel electrophoresis analysis was performed with a native polyacrylamide gel (20%). A Mini-PROTEAN Tetra Cell system (Bio-Rad) was used for the gel electrophoresis with a TBE buffer (Tris base, 44.5 mM; boric acid, 44.5 mM; EDTA, 1 mM). The gels in Figures 4 and 5 were run for 6 h at 60 V in ice. The gel in Figure 2 was run for 5 h at 60 V in ice. All native gels were imaged on a G:Box from Syngene using Genesnap software (Syngene). The gel images were exposed from 300 to 1200 ms. High-resolution melting analysis was performed with a Rotergene Q (Qiagene). For this, 45 μM of the DNA probes was mixed with 10 μM SYBR Green I 10 000× (Invitrogen) in a final volume of 15 μL. The temperature was increased from 25 °C to 98 °C, at a rate of 1 °C per 4 s, and the emission was monitored at 510 nm.

Absorption spectra were recorded on a Perkin-Elmer 1050 UV−vis−NIR with a 2 nm slit width and a data acquisition time of 0.25 s/nm. Circular dichroism spectra were recorded on a Jasco J-815 spectropolarimeter equipped with a CDF-426S Peltier Type CD/fluorescence cell holder maintained at 25 °C. For both the absorption and CD measurements, the samples were measured in quartz cuvettes from Hellma (105250QS10x2mmZ85 mm), volume 200 μL, concentration 15 μM DNA.

The fluorescence decay times have been measured by a time-correlated single photon counting setup described in detail previously.[41] Briefly, the 561 nm pulsed excitation light (8.18 MHz, 1.2 ps full width at half-maximum) was obtained from the frequency-doubled output of an optical parametric oscillator (GWU) pumped by a Ti:sapphire laser (Tsunami, Spectra Physics). The detection system consists of a subtractive double monochromator (9030DS, Sciencetech) and a microchannel plate photomultiplier (R3809U, Hamamatsu). The emission was monitored at 600 nm. A time-correlated single photon counting PC module (SPC 630, Becker & Hickl), which has two constant fraction discriminators, a time-to-amplitude converter, and an analog-to-digital converter on the PC board, was used to obtain the fluorescence decay histograms. The decays were recorded with 5000 counts in the peak channel in time windows of 20 ns (4096 channels) and analyzed by instrument response function deconvolution. The full width at half-maximum of the IRF was typically on the order of 40 ps. The quality of the fits has been judged by the fit parameters χ^2 (<1.2), Z_χ^2 (<3), and the Durbin Watson parameter (1.8 < DW < 2.2) as well as by the visual inspection of the residuals and autocorrelation function as was reported in the literature.[42] All measurements have been performed in Milli-Q water as solvent in 1 cm optical path length disposable PMMA cuvettes (VWR) at an optical density of less than 0.1 at the excitation wavelength.

Conflict of Interest: The authors declare no competing financial interest.

Acknowledgment. S.W.Y. and T.V. gratefully acknowledge financial support from Center for Synthetic Biology at Copenhagen University funded by the UNIK research initiative of the Danish Ministry of Science, Technology and Innovation (grant 09-065274). H.G.K. acknowledges financial support from the Danish Council for Independent Research-Natural Sciences. J.H. acknowledges financial support from the Fonds voor Wetenschappelijk Onderzoek FWO (grants G.0402.09, G.0413.10, G.0697.11), the K. U. Leuven Research Fund (GOA 2011/03), the Flemish government (long-term structural funding: Methusalem funding CASAS METH/08/04), and the Federal Science Policy of Belgium (IAP-VI/27). We thank Thomas Günther-Pomorski for use of his fluorimeter, which is supported by Carlsbergfondet.

Supporting Information Available: Time-dependent evolution of the red AgNC emission (1−5 h). Additional high-resolution melting and gel electrophoresis data. Full spectral excitation and emission scans for the DNA sequences presented in this article. A comparison between a one-, two-, and three-exponential decay curve fit for DNA-GG172-12nt-RED. Salt and pH dependence of red AgNC emission for DNA-12nt-RED-160. This material is available free of charge *via* the Internet at http://pubs.acs.org.

REFERENCES AND NOTES

1. Petty, J. T.; Zheng, J.; Hud, N. V.; Dickson, R. M. DNA-Templated Ag Nanocluster Formation. *J. Am. Chem. Soc.* **2004**, *126*, 5207–5212.
2. Ritchie, C. M.; Johnsen, K. R.; Kiser, J. R.; Antoku, Y.; Dickson, R. M.; Petty, J. T. Ag Nanocluster Formation Using a Cytosine Oligonucleotide Template. *J. Phys. Chem. C* **2007**, *111*, 175–181.
3. Sengupta, B.; Ritchie, C. M.; Buckman, J. G.; Johnsen, K. R.; Goodwin, P. M.; Petty, J. T. Base-Directed Formation of Fluorescent Silver Clusters. *J. Phys. Chem. C* **2008**, *112*, 18776–18782.
4. Sengupta, B.; Springer, K.; Buckman, J. G.; Story, S. P.; Abe, O. H.; Hasan, Z. W.; Prudowsky, Z. D.; Rudisill, S. E.; Degtyareva, N. N.; Petty, J. T. DNA Templates for Fluorescent Silver Clusters and I-Motif Folding. *J. Phys. Chem. C* **2009**, *113*, 19518–19524.
5. Petty, J. T.; Fan, C. Y.; Story, S. P.; Sengupta, B.; Iyer, A. S.; Prudowsky, Z.; Dickson, R. M. DNA Encapsulation of 10 Silver Atoms Producing a Bright, Modulatable, Near-Infrared-Emitting Cluster. *J. Phys. Chem. Lett.* **2010**, *1*, 2524–2529.
6. Petty, J. T.; Sengupta, B.; Story, S. P.; Degtyareva, N. N. DNA Sensing by Amplifying the Number of Near-Infrared Emitting, Oligonucleotide-Encapsulated Silver Clusters. *Anal. Chem.* **2011**, *83*, 5957–5964.
7. Sharma, J.; Yeh, H. C.; Yoo, H.; Werner, J. H.; Martinez, J. S. A Complementary Palette of Fluorescent Silver Nanoclusters. *Chem. Commun.* **2010**, *46*, 3280–3282.
8. Yeh, H. C.; Sharma, J.; Han, J. J.; Martinez, J. S.; Werner, J. H. A DNA-Silver Nanocluster Probe That Fluoresces upon Hybridization. *Nano Lett.* **2010**, *10*, 3106–3110.
9. Gwinn, E. G.; O'Neill, P.; Guerrero, A. J.; Bouwmeester, D.; Fygenson, D. K. Sequence-Dependent Fluorescence of DNA-Hosted Silver Nanoclusters. *Adv. Mater.* **2008**, *20*, 279–283.
10. O'Neill, P. R.; Velazquez, L. R.; Dunn, D. G.; Gwinn, E. G.; Fygenson, D. K. Hairpins with Poly-C Loops Stabilize Four Types of Fluorescent Ag-n:DNA. *J. Phys. Chem. C* **2009**, *113*, 4229–4233.
11. Driehorst, T.; O'Neill, P.; Goodwin, P. M.; Pennathur, S.; Fygenson, D. K. Distinct Conformations of DNA-Stabilized Fluorescent Silver Nanoclusters Revealed by Electrophoretic Mobility and Diffusivity Measurements. *Langmuir* **2011**, *27*, 8923–8933.
12. Zhou, Z.; Du, Y.; Dong, S. DNA-Ag Nanoclusters As Fluorescence Probe for Turn-On Aptamer Sensor of Small Molecules. *Biosens. Bioelectron.* **2011**, *28*, 33–37.

13. Yang, S. W.; Vosch, T. Rapid Detection of MicroRNA by a Silver Nanocluster DNA Probe. *Anal. Chem.* **2011**, *83*, 6935–6939.
14. Petty, J. T.; Story, S. P.; Juarez, S.; Votto, S. S.; Herbst, A. G.; Degtyareva, N. N.; Sengupta, B. Optical Sensing by Transforming Chromophoric Silver Clusters in DNA Nanoreactors. *Anal. Chem.* **2011**, *84*, 356–364.
15. Pal, S.; Varghese, R.; Deng, Z.; Zhao, Z.; Kumar, A.; Yan, H.; Liu, Y. Site-Specific Synthesis and *in Situ* Immobilization of Fluorescent Silver Nanoclusters on DNA Nanoscaffolds by Use of the Tollens Reaction. *Angew. Chem.* **2011**, *123*, 4262–4265.
16. Neidig, M. L.; Sharma, J.; Yeh, H.-C.; Martinez, J. S.; Conradson, S. D.; Shreve, A. P. Ag K-Edge EXAFS Analysis of DNA-Templated Fluorescent Silver Nanoclusters: Insight into the Structural Origins of Emission Tuning by DNA Sequence Variations. *J. Am. Chem. Soc.* **2011**, *133*, 11837–11839.
17. Li, T.; Zhang, L. B.; Ai, J.; Dong, S. J.; Wang, E. K. Ion-Tuned DNA/Ag Fluorescent Nanoclusters As Versatile Logic Device. *ACS Nano* **2011**, *5*, 6334–6338.
18. Kun, M. Q. C.; Liu, G.; Wu, F.; Xu, S.; Shao, Y. DNA Abasic Site-Directed Formation of Fluorescent Silver Nanoclusters for Selective Nucleobase Recognition. *Nanotechnology* **2011**, *22*, 305502.
19. Huang, Z.; Pu, F.; Lin, Y.; Ren, J.; Qu, X. Modulating DNA-Templated Silver Nanoclusters for Fluorescence Turn-On Detection of Thiol Compounds. *Chem. Commun.* **2011**, *47*, 3487–3489.
20. Huang, Z.; Pu, F.; Hu, D.; Wang, C.; Ren, J.; Qu, X. Site-Specific DNA-Programmed Growth of Fluorescent and Functional Silver Nanoclusters. *Chem.—Eur. J.* **2011**, *17*, 3774–3780.
21. Fu, Y.; Zhang, J.; Chen, X.; Huang, T.; Duan, X.; Li, W.; Wang, J. Silver Nanomaterials Regulated by Structural Competition of G-/C-Rich Oligonucleotides. *J. Phys. Chem. C* **2011**, *115*, 10370–10379.
22. Deng, L.; Zhou, Z.; Li, J.; Li, T.; Dong, S. Fluorescent Silver Nanoclusters in Hybridized DNA Duplexes for the Turn-On Detection of Hg^{2+} Ions. *Chem. Commun.* **2011**, *47*, 11065–11067.
23. Antoku, Y.; Hotta, J.-i.; Mizuno, H.; Dickson, R. M.; Hofkens, J.; Vosch, T. Transfection of Living HeLa Cells with Fluorescent Poly-Cytosine Encapsulated Ag Nanoclusters. *Photochem. Photobiol. Sci.* **2010**, *9*, 716–721.
24. Richards, C. I.; Hsiang, J. C.; Senapati, D.; Patel, S.; Yu, J.; Vosch, T.; Dickson, R. M. Optically Modulated Fluorophores for Selective Fluorescence Signal Recovery. *J. Am. Chem. Soc.* **2009**, *131*, 4619–4621.
25. Patel, S. A.; Cozzuol, M.; Hales, J. M.; Richards, C. I.; Sartin, M.; Hsiang, J. C.; Vosch, T.; Perry, J. W.; Dickson, R. M. Electron Transfer-Induced Blinking in Ag Nanodot Fluorescence. *J. Phys. Chem. C* **2009**, *113*, 20264–20270.
26. Vosch, T.; Antoku, Y.; Hsiang, J. C.; Richards, C. I.; Gonzalez, J. I.; Dickson, R. M. Strongly Emissive Individual DNA-Encapsulated Ag Nanoclusters As Single-Molecule Fluorophores. *Proc. Natl. Acad. Sci. U. S. A.* **2007**, *104*, 12616–12621.
27. Patel, S. A.; Richards, C. I.; Hsiang, J. C.; Dickson, R. M. Water-Soluble Ag Nanoclusters Exhibit Strong Two-Photon-Induced Fluorescence. *J. Am. Chem. Soc.* **2008**, *130*, 11602–11603.
28. Choi, S. M.; Yu, J. H.; Patel, S. A.; Tzeng, Y. L.; Dickson, R. M. Tailoring Silver Nanodots for Intracellular Staining. *Photochem. Photobiol. Sci.* **2011**, *10*, 109–115.
29. Guo, W. W.; Yuan, J. P.; Wang, E. K. Oligonucleotide-Stabilized Ag Nanoclusters As Novel Fluorescence Probes for the Highly Selective and Sensitive Detection of the Hg^{2+} Ion. *Chem. Commun.* **2009**, 3395–3397.
30. Guo, W. W.; Yuan, J. P.; Dong, Q. Z.; Wang, E. K. Highly Sequence-Dependent Formation of Fluorescent Silver Nanoclusters in Hybridized DNA Duplexes for Single Nucleotide Mutation Identification. *J. Am. Chem. Soc.* **2010**, *132*, 932–934.
31. Richards, C. I.; Choi, S.; Hsiang, J. C.; Antoku, Y.; Vosch, T.; Bongiorno, A.; Tzeng, Y. L.; Dickson, R. M. Oligonucleotide-Stabilized Ag Nanocluster Fluorophores. *J. Am. Chem. Soc.* **2008**, *130*, 5038–5039.
32. Chen, X. A MicroRNA As a Translational Repressor of *APETALA2* in *Arabidopsis* Flower Development. *Science* **2004**, *303*, 2022–2025.
33. Ai, J.; Guo, W.; Li, B.; Li, T.; Li, D.; Wang, E. DNA G-Quadruplex-Templated Formation of the Fluorescent Silver Nanocluster and Its Application to Bioimaging. *Talanta* **2012**.
34. Vallone, P. M.; Butler, J. M. AutoDimer: A Screening Tool for Primer-Dimer and Hairpin Structures. *Biotechniques* **2004**, *37*, 226–231.
35. Zuker, M. Mfold Web Server for Nucleic Acid Folding and Hybridization Prediction. *Nucleic Acids Res.* **2003**, *31*, 3406–3415.
36. Ono, A.; Cao, S.; Togashi, H.; Tashiro, M.; Fujimoto, T.; Machinami, T.; Oda, S.; Miyake, Y.; Okamoto, I.; Tanaka, Y. Specific Interactions Between Silver(I) Ions and Cytosine-Cytosine Pairs in DNA Duplexes. *Chem. Commun.* **2008**, 4825–4827.
37. Wang, Y.; Li, J.; Wang, H.; Jin, J.; Liu, J.; Wang, K.; Tan, W.; Yang, R. Silver Ions-Mediated Conformational Switch: Facile Design of Structure-Controllable Nucleic Acid Probes. *Anal. Chem.* **2010**, *82*, 6607–6612.
38. Lan, G. Y.; Chen, W. Y.; Chang, H. T. One-Pot Synthesis of Fluorescent Oligonucleotide Ag Nanoclusters for Specific and Sensitive Detection of DNA. *Biosens. Bioelectron.* **2011**, *26*, 2431–2435.
39. Schultz, D.; Gwinn, E. Stabilization of Fluorescent Silver Clusters by RNA Homopolymers and Their DNA Analogs: C, G *versus* A,T(U) Dichotomy. *Chem. Commun.* **2011**, *47*, 4715–4717.
40. Wu, J.; Fu, Y.; He, Z.; Han, Y.; Zheng, L.; Zhang, J.; Li, W. Growth Mechanisms of Fluorescent Silver Clusters Regulated by Polymorphic DNA Templates: A DFT Study. *J. Phys. Chem. B* **2012**, *116*, 1655–1665.
41. Maus, M.; Rousseau, E.; Cotlet, M.; Schweitzer, G.; Hofkens, J.; Van der Auweraer, M.; De Schryver, F. C.; Krueger, A. New Picosecond Laser System for Easy Tunability over the Whole Ultraviolet/Visible/Near Infrared Wavelength Range Based on Flexible Harmonic Generation and Optical Parametric Oscillation. *Rev. Sci. Instrum.* **2001**, *72*, 36–40.
42. Boens, N.; Qin, W. W.; Basaric, N.; Hofkens, J.; Ameloot, M.; Pouget, J.; Lefevre, J. P.; Valeur, B.; Gratton, E.; Vandeven, M.; *et al.* Fluorescence Lifetime Standards for Time and Frequency Domain Fluorescence Spectroscopy. *Anal. Chem.* **2007**, *79*, 2137–2149.